

New insights into the structure and reduction of graphite oxide

Wei Gao¹, Lawrence B. Alemany¹, Lijie Ci² and Pulickel M. Ajayan^{1,2*}

Graphite oxide is one of the main precursors of graphene-based materials, which are highly promising for various technological applications because of their unusual electronic properties. Although epoxy and hydroxyl groups are widely accepted as its main functionalities, the complete structure of graphite oxide has remained elusive. By interpreting spectroscopic data in the context of the major functional groups believed to be present in graphite oxide, we now show evidence for the presence of five- and six-membered-ring lactols. On the basis of this chemical composition, we devised a complete reduction process through chemical conversion by sodium borohydride and sulfuric acid treatment, followed by thermal annealing. Only small amounts of impurities are present in the final product (less than 0.5 wt% of sulfur and nitrogen, compared with about 3 wt% with other chemical reductions). This method is particularly effective in the restoration of the π -conjugated structure, and leads to highly soluble and conductive graphene materials.

Graphene—a single layer of sp^2 -hybridized carbon atoms found in graphite—is now well known for its unusual electronic properties and possible applications in various fields. Nevertheless, several of these applications are still not feasible because the large-scale production of pure graphene sheets remains challenging. The chemical reduction of graphite oxide (GO) is one of the established procedures to make graphene in large volume. Many primary products with either high conductivity or good solubility have been made by chemical reduction, intercalation or thermal annealing, but most of these procedures create either highly functionalized materials ($\sim 3\%$ heteroatoms other than O)^{1,2} or materials with a surface polymer coating³. Liquid-phase exfoliation of graphite turns out to be a facile way to make graphene, but yields are quite low ($\sim 1\text{ wt}\%$)⁴. Above all, fabrication of single-layer graphene with high conductivity, low functionality and high solubility has not yet been achieved on a large scale.

Among all the strategies pursued, the reduction of GO might be one of the most promising routes; however, the reduction mechanism remains ambiguous and the detailed structure of GO is unclear. Interest in the structure of GO has increased recently, and the most probable structural models are given by the Lerf–Klinowski model⁵ and the Dékány model⁶. The final structure of GO obtained depends on the chemical oxidation process used, and hence the two models differ considerably. We have used the oxidation protocol that results in the material that is typically described by the Lerf–Klinowski model, and hence we will consider this as our base structure model of GO here. However, even this model cannot explain all the features observed in experiments, and some of the functionalities remain to be defined. Here we offer experimental support for a peripheral structure for GO containing five- and six-membered-ring lactols (Fig. 1b) and possibly an occasional 2-hydroxynaphthalic anhydride or 1,3-dihydroxyxanthone (Supplementary Information). Graphite oxide produced by a modified Hummers method (see Methods) is found to be quite hydrophilic. It is easily dispersed in water with an average sheet size of around $1\ \mu\text{m}$ and average thickness of around $1\ \text{nm}$ (Fig. 1a, Supplementary Fig. S2).

Results and discussion

Chemical composition of the graphite oxide sheets. Various solid-state ^{13}C NMR experiments were performed on our GO sample (Fig. 2 and Supplementary Figs S7 and S8). The principal features are clearly in good agreement with spectra shown in the literature and are discussed in detail in the Supplementary Information. The direct ^{13}C pulse spectrum (Fig. 2a) is very similar to the direct ^{13}C pulse spectrum recently reported by Cai *et al.*⁷ in their preparation of highly ^{13}C -enriched graphite oxide. As in our work, Blumenfeld *et al.*⁸ detected noticeably stronger signals around 100 and 170 ppm in a direct ^{13}C pulse spectrum than in a ^1H - ^{13}C cross polarization (CP) spectrum.

These appear to be the only other studies of GO that have detected a signal near 100 ppm. A comparison of the intensity of this signal in a CP spectrum and the intensity in a CP experiment with dipolar dephasing led Cai *et al.*⁷ to conclude that it resulted from non-protonated carbons, but no further assignment has been indicated^{7,8}. The corresponding comparisons of the CP spectra in Supplementary Fig. S7a,c and of the direct ^{13}C pulse spectra in Supplementary Figs S7d,e also lead to the conclusion that the signal at 101 ppm results from non-protonated carbons. Appropriately substituted five- and six-membered-ring lactols along the periphery^{9–11} are the most likely structures in GO to be responsible for this signal; 2-hydroxynaphthalic anhydrides or 1,3-dihydroxyxanthenes might be minor contributing structures, as discussed in the Supplementary Information. The lactol moieties have previously been considered as possible structural elements in acidic carbon surface oxides^{9–11}, with only indirect evidence for their presence⁹.

Five- or six-membered-ring lactols, 2-hydroxynaphthalic anhydrides, and 1,3-dihydroxyxanthenes will, of course, also give signals in the carbonyl region. The signals observed in this work (Fig. 2a) and other work^{1,7,8,12} at 167–170 ppm are certainly consistent with an ester carbonyl. For reference, we note that the carbonyl carbon in the seven-membered-ring lactol generated by oxidation of pyrene (see Supplementary Information) gives a signal at 167.4 ppm (ref. 13). The intensity near 167 ppm is clearly stronger than the intensity near 100 ppm, so it is possible that there is some other contribution to this signal in addition to

¹Department of Chemistry, ²Department of Mechanical Engineering and Materials Science, Rice University, Houston, Texas 77005, USA.

*e-mail: ajayan@rice.edu

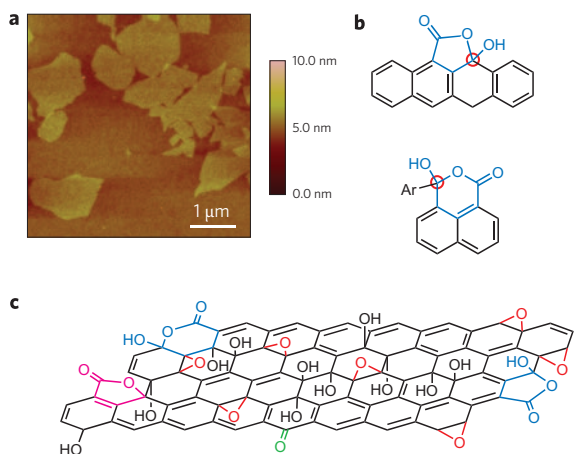


Figure 1 | AFM image and structural model of the graphite oxide (GO) sheets. **a**, An AFM image of GO sheets on a silicon substrate. **b**, Structure of the five- and six-membered lactol rings. The carbons circled in red are those that give ^{13}C NMR signals at 101 ppm. **c**, New structural model of GO, taking into account the five- and six-membered lactol rings (blue), ester of a tertiary alcohol (purple), hydroxyl (black), epoxy (red) and ketone (green) functionalities. The relative ratios are likely to be 115 (hydroxyl and epoxy): 3 (lactol O–C–O): 63 (graphitic sp^2 carbon): 10 (lactol + ester + acid carbonyl): 9 (ketone carbonyl) (see Supplementary Information for details). The model here only shows the chemical connectivity, and not the steric orientation, of these functionalities.

lactols. The presence of numerous tertiary alcohols in GO allows for the possibility of some of them reacting with nearby carboxylic acids on the periphery (either on the same graphene sheet or an adjacent sheet) to generate an ester. Such ester carbonyl signals also appear near 167 ppm, as shown by the data for *t*-butyl benzoate in CDCl_3 (165.6 ppm) (ref. 14), 1-adamantyl benzoate in CDCl_3 (165.3 ppm) (ref. 15), and *t*-butyl 9-anthroate in CDCl_3 (169.0 ppm) (ref. 16). The signals observed in this and other work⁷ at 191 and 193 ppm can reasonably be attributed only to carbonyl groups, most likely ketones. Their precise nature is not yet clear, but these signals do not appear to result from simple polycyclic aromatic ketones (for example, benzanthrone, naphanthrone, and other five-ring aromatic ketones), as the carbonyl carbon signals for solutions of these in CDCl_3 range from 184–186 ppm (refs 17,18). Hydroxyl and epoxy groups near the ketone carbonyl groups (in an as yet unknown functionalization pattern) most likely account for the downfield shift to about 192 ppm. The majority of the functional groups in GO are therefore still thought to be epoxy and hydroxyl groups (Fig. 1c).

Two-step reduction process. On the basis of the chemical composition described above, we have developed a two-step reduction process—deoxygenation with NaBH_4 , followed by dehydration with concentrated sulfuric acid—that is really simple and effective in the restoration of graphene structure. Compared with other reported routes, including hydrazine reduction or direct GO thermal annealing, our strategy is far better as it produces graphene with a very low number of remaining functional groups, high conductivity, larger crystallite size and good solubility. In addition, our new procedure does not involve the highly toxic reagent hydrazine or dimethylhydrazine, thus providing a more environmentally friendly protocol. A schematic illustration of the typical procedure proposed here is shown in Fig. 3a. The GO structure is the same as the one we have established above, which is a modified version of the Lerf–Klinowski model. The structure of the product obtained at every step is deduced from the solid state ^{13}C NMR spectra as well as from X-ray photoelectron spectroscopy (XPS) analysis.

Characterization of the reduced products. Treating GO with NaBH_4 causes an enormous structural change (product CCG1; chemically converted graphene 1). The signal for graphitic sp^2 carbon dominates both the CP and the direct ^{13}C pulse spectra (Fig. 2b). This signal is shifted upfield by 11 ppm (expanded plots of the spectra before and after NaBH_4 treatment are shown in Supplementary Fig. S8 to facilitate comparison). The CP and direct ^{13}C pulse spectra of CCG1 show essentially complete elimination of all epoxides (60 ppm region), almost as large a decrease in the alcohol content (70 ppm region), complete elimination of all ketones (190 ppm region), the apparent elimination of all lactols (no shoulder recognizable in the 100 ppm region, much less intensity near 167 ppm), and the apparent elimination of any esters (again, much less intensity near 167 ppm).

The intensity of a new signal at about 175 ppm in the direct ^{13}C pulse spectrum is clearly less than that of each of the carbonyl signals before NaBH_4 treatment. This new signal might result from aromatic carboxylic acids, which are known to give a signal in this region (benzoic acid in CDCl_3 at 172.4 ppm (ref. 19), *m*-toluic acid in CDCl_3 at 172.8 ppm (ref. 20), and biphenyl-2-carboxylic acid in CDCl_3 at 174.1 ppm (Spectral Database for Organic Compounds, http://riodb01.ibase.aist.go.jp/sdbs/cgi-bin/cre_index.cgi?lang=eng, compound #12557)) and to be resistant to reduction by NaBH_4 (ref. 21). Any carboxyl signals in the precursor GO would be harder to recognize because of the presence of other carbonyl groups and because the numerous hydroxyl and epoxy groups present in GO would presumably shift the carboxyl carbon signal from the region near 173–174 ppm typical of simple aromatic carboxylic acids. Treatment with NaBH_4 also generates some very shielded aliphatic signals whose origin is not clear.

The NaBH_4 reduction product CCG1 is considerably more like graphite, with a conductivity 200 times higher than the precursor GO. A spectrum similar to that given by sample CCG1 has been reported¹ for a sample of GO reduced with NaBH_4 and then sulfonated¹. For the reasons discussed in the analysis of the CP and direct ^{13}C pulse spectra of GO (see Supplementary Information), the direct ^{13}C pulse spectrum of CCG1 is much more meaningful than the CP spectrum.

Subsequent treatment of CCG1 with H_2SO_4 increases the conductivity by another factor of 20 by eliminating the small amount of aliphatic functionality and leaving only graphitic sp^2 carbon and some carbonyl carbon in product CCG2 (Fig. 2b). The carbonyl carbon is more evident in the CP spectrum. Acid treatment apparently caused the remaining tertiary alcohols to dehydrate to form alkenes that are part of a graphitic sp^2 carbon network with protons and carboxylic acid groups on the periphery. The treatment with H_2SO_4 results in a small additional upfield shift of the graphitic carbon signal (to 119 ppm), which also broadens noticeably, thereby reducing the signal to noise ratio, even with many more pulses than in the corresponding spectrum of the NaBH_4 reduction product. Spectra similar to that given by sample CCG2 have been reported for a sample of GO reduced with NaBH_4 , sulfonated, and then reduced with hydrazine¹ and for a sample of GO reduced with hydrazine hydrate²².

Subsequent annealing of CCG2 in Ar/H_2 at 1,100 °C for 15 minutes increases the conductivity by another factor of 12 and causes the sample (product CCG3) to behave very differently in the NMR magnet. More pressure than normal was required to spin the rotor, and tuning and matching the ^{13}C and ^1H channels in the probe proved much more difficult; indeed, the ^1H channel could not be adequately adjusted, as the tuning and matching adjustments needed exceeded the probe's range. Not surprisingly, the resulting CP spectrum was only noise (Fig. 2b), and the direct ^{13}C pulse spectrum exhibited only a broad, relatively weak signal shifted even further upfield, with a maximum at about 105 ppm

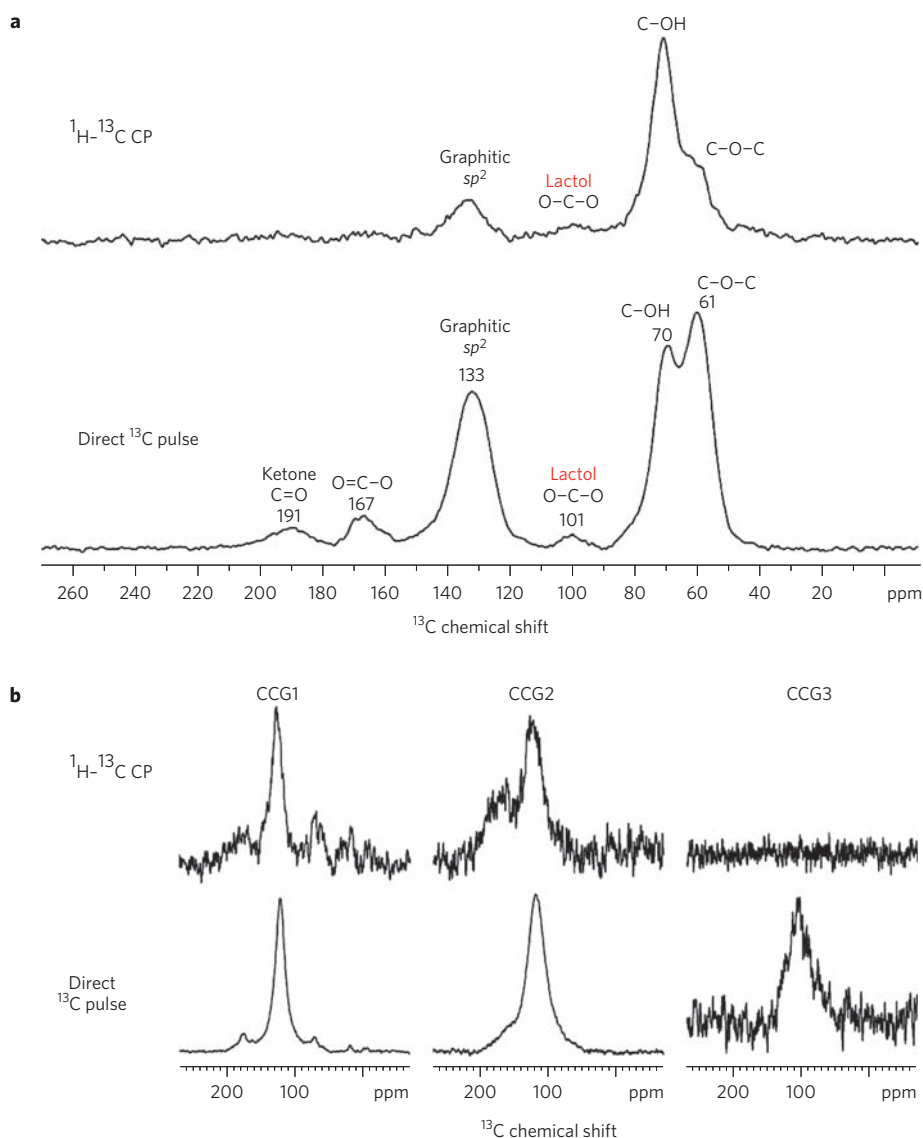


Figure 2 | Solid-state ^{13}C magic-angle spinning (MAS) NMR spectra of GO and its reduction products. **a**, A ^1H - ^{13}C cross polarization (CP) spectrum of GO obtained with 7.6 kHz MAS and a contact time of 1 ms (67,000 scans), and a direct ^{13}C pulse spectrum obtained with 12 kHz MAS and a 90° ^{13}C pulse (10,000 scans). The peak at 101 ppm is caused by the carbons of five- and six-membered-ring lactols highlighted in red in Fig. 1b. **b**, CPMAS and direct ^{13}C pulse MAS spectra of reduction products CCG1, CCG2 and CCG3 (with 25,320, 17,000, and 3,600 scans, respectively, in the CP spectra and 10,600, 24,000, and 6,800 scans, respectively, in the direct ^{13}C pulse spectra). Note that higher than normal drive pressure was required to spin sample CCG3 at 7.6 kHz for the CP experiment and that a drive pressure that would normally spin a sample at 12 kHz caused sample CCG3 to spin at only 9.4 kHz. A series of processing steps removes the aliphatic functional groups and significantly broadens and shifts the aromatic signal of the extended graphitic sp^2 carbon network that is generated.

(Fig. 2b). Clearly, annealing generated a sample even more like pure graphite, for which sample spinning and probe tuning are even more problematic and for which a ^{13}C NMR signal cannot be obtained even in a direct ^{13}C pulse experiment.

Electrical conductivity of the reduced products is another important criterion to evaluate how the π conjugated system has been restored in this structure. Original GO is an insulator, with a conductivity of around 0.5 S m^{-1} . The four orders of magnitude increase in conductivity after reduction here clearly indicates an efficient restoration of the π -conjugated system in our product, induced by the deoxygenation and dehydration. NaBH_4 de-oxygenation is necessary in our procedure; in the control experiment when only concentrated H_2SO_4 was used, the conductivity obtained was only 46.4 S m^{-1} . Annealing of CCG2 at $1,100^\circ\text{C}$ led to a further increase in conductivity up to $2.02 \times 10^4 \text{ S m}^{-1}$, which is on the same order

of magnitude as graphite powder. The conductivity here was measured by a standardized ‘four-point probe’ setup (Fig. S1 in Supplementary Information) in order to eliminate contact resistance, and each sample pellet was cut into rectangular shape and measured three times to obtain an average value.

Consistent with the ^{13}C NMR spectra, high-resolution carbon 1s peaks in XPS (Fig. 3b) also indicated good restoration of $\text{C}=\text{C}$ bonds, as well as the existence of carbonyl groups in the final product. The original GO signal shows two separated peaks, as expected, due to the high percentage of oxygen functionalities. After reduction, $\text{C}=\text{C}$ bonds dominate, as shown by one single peak with small tails at the higher binding energy region. The small bump around 288.5 eV in the CCG2 curve is within the ketone and carboxyl carbon region. The π to π^* satellite peak around 291 eV was observed both in CCG3 and graphite powder

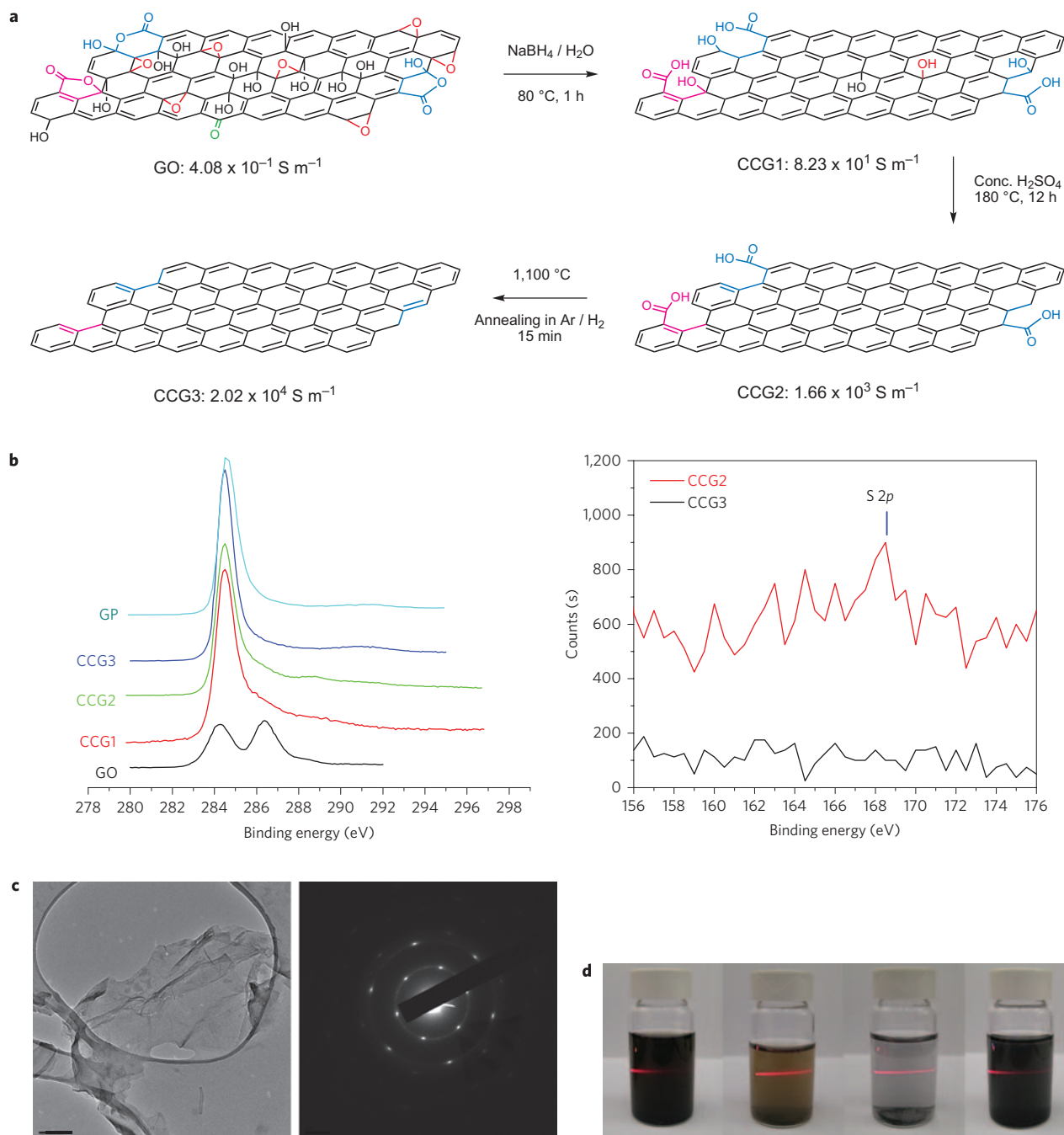


Figure 3 | Schematic representation of the GO reduction procedure and characterization of the products obtained. **a**, The two-step reduction process, followed by the annealing treatment, is an effective method to convert GO sheets into graphene-based materials (where CCG stands for chemically converted graphene). **b,c**, XPS and TEM characterizations indicate good restoration of the graphene structure, as well as little sulfur remaining in the final product. **b**, Left: XPS analysis of carbon 1s in different samples. Each curve was obtained by 25 scans at high sensitivity. Right: XPS signal of sulfur 2p from 156 to 176 eV (45° takeoff angle, 200 μm beam size). **c**, Left: TEM image of CCG2. Right: corresponding selected area electron diffraction pattern taken at the relatively flat edge of the graphene sheet. **d**, Solubility tests. From left to right: GO in deionized water; GO in DMF; CCG3 in deionized water; CCG3 in DMF after 50 minutes water bath sonication. A red laser beam was directed through the dispersions to show the Tyndall effect of these colloidal solutions. Although GO is more soluble in water than in DMF, after reduction the product CCG3 is more soluble in DMF than in water. This is consistent with its hydrophobic nature.

curves, which indicates that the delocalized π conjugation is restored in our sample. Furthermore, the atomic composition (wt%) of all the samples was analysed by both XPS and elemental analysis. Both Fig. 3b and Supplementary Table S1 show that there is little sulfur (<0.518 wt%) or nitrogen (<0.5 wt%) left in the final product CCG3, making our product distinct from the other CCGs, such as a hydrazine reduction product

(N wt% \approx 3.25%)² and sulfonation products (S mole% \approx 2.8%, N mole% \approx 3.2%)¹. The oxygen percentage (12.68 wt%) in CCG2 is close to the value reported by others^{1,2}. Oxygen might be coming from two possible structures in CCG2: the chemically adsorbed water and the carboxyl functionalities remaining in this structure. After annealing, the oxygen content in CCG3 becomes less than 0.5 wt%, which is close to the value in graphite powder.

In comparison, literature reports show that when GO is directly annealed at up to 1,050 °C in Ar atmosphere, the oxygen content remains as high as ~9.3% (ref. 23). A transmission electron microscope (TEM) image of CCG2 was also obtained (Fig. 3c). Unfortunately, but reasonably, most of the sheets aggregated into thicker flakes with a wide distribution of sizes, ranging from 200 nm to 2 µm. Unlike the flakes that peel off from highly ordered pyrolytic graphite, these sheets aggregated in a disordered manner; thus, on the periphery of these flakes, monolayer graphene sheets were frequently observed. The selected area electron diffraction pattern (Fig. 3c) here clearly indicates the graphitic crystalline structure. Furthermore, the relative intensity of the inner and outer circle spots was found to be ~1, corresponding to a 'single layer' graphene structure. Thermogravimetric analysis (TGA) data of all the samples are available in the Supplementary Information (Fig. S3).

We were able to obtain stable suspensions of sample CCG3 in DMF. After 50 minutes of sonication, the suspension remained stable for at least several weeks. Figure 3d shows a comparison of solubility for GO and CCG3 in deionized water and dimethylformamide (DMF) separately. GO shows higher solubility in water than in DMF, owing to the hydroxyl, epoxy and carboxyl functionalities on its surface. After reduction, the product shows higher solubility in DMF than in water, which is reasonable, given its hydrophobic nature. This is quite different from CCGs reported in the literature^{1,2}, as most of them maintain high solubility in water rather than in DMF. Tyndall scattering was shown by directing a red laser beam through each suspension to indicate the colloidal nature of the mixtures.

Conclusions

Interpreting solid state ¹³C NMR spectra in the context of the major functional groups believed to be present in GO results in five- and six-membered-ring lactols along the periphery of the layers being proposed as the most likely functional groups responsible for the minor, but significant, signal near 100 ppm 2-hydroxynaphthalic anhydrides and 1,3-dihydroxyxanthenes appear to contribute to only a very limited extent (if at all) to this signal. The functionalized anhydride could easily be accommodated along the periphery of a sheet, but a functionalized xanthone would require an interior defect site in the graphene structure in order to accommodate the six-membered-ring ether functionality.

In principle, 1,3-dihydroxyxanthenes and 2-hydroxynaphthalic anhydrides could be differentiated from lactols through a two-dimensional solid state ¹³C NMR experiment detecting scalar-coupled pairs of ¹³C nuclei^{24–28}. 1,3-Dihydroxyxanthenes and 2-hydroxynaphthalic anhydrides would exhibit a distinctive coupling between the carbonyl carbon and the adjacent enolic carbon (at about 100 ppm), whereas lactols would exhibit a coupling between the O–C–O carbon (at about 100 ppm) and the two adjacent non-carbonyl carbons. Such an experiment would require preparing GO with ¹³C-enriched graphite⁷ and appears to be the most secure method²⁷ for definitively assigning the signal near 100 ppm.

In this context, it is worth noting that in the study by Cai *et al.*⁷, a ¹³C–¹³C dipolar recoupling experiment (that is, exploiting through-space rather than through-bond coupling) applied to ¹³C-enriched GO demonstrated the spatial proximity of the ¹³C nuclei giving signals at about 101 ppm to the ¹³C nuclei giving signals at 60–70 ppm. An epoxide group adjacent to a lactol would apparently have essentially no effect on the lactol O–C–O chemical shift (see Supplementary Information). However, the dipolar recoupling experiment did not detect any signals that could provide information on the spatial environment of the signals with comparable intensities at 169 and 193 ppm, which led the authors to conclude that these ¹³C nuclei 'are spatially separated from a majority of

the *sp*², C–OH, and epoxide carbons⁷. It is hard to envision just what the environment of these nuclei would then be. Indeed, Cai *et al.* concluded that 'further studies would be needed to define all of the structural details of the system'⁷.

The two-dimensional solid state ¹³C NMR experiment detecting scalar-coupled pairs of ¹³C nuclei might also provide information on the functional groups near the ketone carbonyl carbon believed to be responsible for the signal at 191 ppm and on the functional groups near the carbonyl groups responsible for the signal at 167 ppm. In general, this experiment could potentially better define the structure of GO by providing much information on the specific types of functional groups on the periphery of the GO sheets, which is clearly important as about 11% of the carbon is in the signals near 100, 167, and 191 ppm (Supplementary Information). However, even with this uncertainty as to some of the structural details, our two-step reduction strategy yields nearly pure graphene that is highly conductive, has very few functional groups and no polymer coating, and is soluble in DMF. This procedure offers an alternative route to large-scale graphene production for applications that require such material.

Methods

Synthesis of GO and its reduction. The starting material is commercially available graphite powder (SP-1 graphite, purchased from Bay Carbon Corporation). GO was obtained by harsh oxidation of the graphite powder according to the modified Hummers method^{29,30}. After purification, the product was put in a vacuum desiccator over phosphorous pentoxide for a week. The dry GO sample was used for X-ray diffraction (XRD), Fourier transform infrared (FTIR) spectroscopy, atomic force microscopy (AFM), Raman spectroscopy, NMR spectroscopy and XPS analysis. For the reduction procedure, dry GO was dispersed in deionized water (18 MΩ, Purelab Classic) to give a 1.0 g l⁻¹ colloidal solution. The pH of this solution was adjusted to 9~10 by 5 wt% sodium carbonate solution. Sodium borohydride (800 mg, reagent grade, 98.5%, Sigma-Aldrich) was directly added into 100 ml GO dispersion under magnetic stirring, and the mixture was kept at 80 °C for 1 h with constant stirring¹. The reduction product was separated by filtration and washed with large amounts of water several times to remove most residual ions. This partially reduced GO was kept in a vacuum desiccator with phosphorous pentoxide for two days and redispersed in concentrated sulfuric acid (UN 1830, reagent grade, Fisher Scientific) and heated to 120 °C with stirring for 12 h. After cooling down, the dispersion was diluted with deionized water. The final product was separated by filtration and thoroughly rinsed with water to remove most impurities. The product powder was compressed into a pellet and further annealed at 1,100 °C under 1.3 standard litre per minute gas flow of Ar with 15 vol% H₂ for 15 minutes.

Analytical instrumentation. Solid state ¹³C magic-angle spinning (MAS) NMR spectra were acquired on a Bruker Avance-200 spectrometer (50.3 MHz ¹³C, 200.1 MHz ¹H) using standard Bruker pulse programs, as described previously³¹, as well as a modified pulse program in order to incorporate dipolar dephasing into the direct ¹³C pulse experiment. Additional NMR details are given in the Supplementary Information and in Fig. 2 and Supplementary Figs S7–9. The powder samples were compressed into pellets under 4,000 psi pressure (4350.L, Carver) with thicknesses of around several hundred micrometres and bulk densities of around 1.1 g cm⁻³, and conductivity was measured by a fixed 'film four-point probe' setup (Supplementary Fig. S1). Raman spectra (Supplementary Fig. S6) were recorded with a Renishaw InVia Raman microscope using a ×50 objective lens at room temperature, with a 514.5 nm laser beam and 1,800 lines per mm grating. The AFM image (Fig. 1 and Supplementary Fig. S2) was obtained on a Digital Instrument Nanoscope IIIA AFM. The TEM image (Fig. 3c) and the selected area electron diffraction pattern (Fig. 3c) were obtained on a JEOL 2100 Field Emission Gun TEM. XPS analyses (Fig. 3b) were carried out on a PHI Quanterra X-Ray photoluminescence spectrometer with a chamber pressure of 5 × 10⁻⁹ torr and an Al cathode as the X-ray source. The source power was set at 100 W, and pass energies of 140.00 eV for survey scans and 26.00 eV for high-resolution scans were used. XRD data (Supplementary Fig. S5) were collected on a Rigaku D/Max Ultima II Powder X-ray diffractometer. FTIR spectra (Supplementary Fig. S4) were obtained on a Nicolet FTIR Microscope with an MCT/A detector, and for TGA-FTIR measurements, an MCT/B detector was used. TGA (Supplementary Fig. S3) was carried out on an SDT 2960 Simultaneous DSC-TGA, TA Instrument. For Raman, XPS, XRD and FTIR measurements, solid powder samples were used. Elemental analyses were performed by Galbraith Laboratories.

Received 29 April 2009; accepted 3 June 2009;
published online 5 July 2009

References

1. Si, Y. & Samulski, E. T. Synthesis of water soluble graphene. *Nano Lett.* **8**, 1679–1682 (2008).
2. Li, D., Müller, M. B., Gilje, S., Kaner, R. B. & Wallace, G. G. Processable aqueous dispersions of graphene nanosheets. *Nature Nanotech.* **3**, 101–105 (2008).
3. Li, X. *et al.* Highly conducting graphene sheets and Langmuir-Blodgett films. *Nature Nanotech.* **3**, 538–542 (2008).
4. Hernandez, Y. *et al.* High-yield production of graphene by liquid-phase exfoliation of graphite. *Nature Nanotech.* **3**, 563–568 (2008).
5. Lerf, A., He, H., Forster, M. & Klinowski, J. Structure of graphite oxide revisited. *J. Phys. Chem. B* **102**, 4477–4482 (1998).
6. Szabó, T. *et al.* Evolution of surface functional groups in a series of progressively oxidized graphite oxides. *Chem. Mater.* **18**, 2740–2749 (2006).
7. Cai, W. *et al.* Synthesis and solid-state NMR structural characterization of ^{13}C -labeled graphite oxide. *Science* **321**, 1815–1817 (2008).
8. Blumenfeld, A. L., Muradyan, V. E., Shumilova, I. B., Parnes, Z. N. & Novikov, Y. N. Investigation of graphite oxide by means of ^{13}C NMR and ^1H spin-lattice relaxation. *Mater. Sci. Forum* **91–93**, 613–617 (1992).
9. Boehm, H. P., Diehl, E., Heck, W. & Sappok, R. Surface oxides of carbon. *Angew. Chem. Int. Ed.* **3**, 669–677 (1964).
10. Boehm, H. P. Some aspects of the surface chemistry of carbon blacks and other carbons. *Carbon* **32**, 759–769 (1994).
11. Fuente, E., Menéndez, J. A., Díez, M. A., Suárez, D. & Montes-Morán, M. A. Infrared spectroscopy of carbon materials: a quantum chemical study of model compounds. *J. Phys. Chem. B* **107**, 6350–6359 (2003).
12. Wang, Z. M., Hoshino, K., Shishibori, K., Kanoh, H. & Ooi, K. Surfactant-mediated synthesis of a novel nanoporous carbon-silica composite. *Chem. Mater.* **15**, 2926–2935 (2003).
13. Gillis, R. G. & Porter, Q. N. 5-Methoxyphenanthrene-4-carboxylic acid. *Aust. J. Chem.* **42**, 1007–1010 (1989).
14. Pelletier, S. W., Djarmati, Z. & Pape, C. Substituent effects in ^{13}C NMR Spectroscopy: methyl, ethyl, 2-propyl and 2-methyl-2-propyl carboxylates. *Tetrahedron* **32**, 995–996 (1976).
15. Mukaiyama, T., Shintou, T. & Fukumoto, K. A convenient method for the preparation of inverted *tert*-alkyl carboxylates from chiral *tert*-alcohols by a new type of oxidation-reduction condensation using 2,6-dimethyl-1,4-benzoquinone. *J. Am. Chem. Soc.* **125**, 10538–10539 (2003).
16. Sweeting, L. M. *et al.* Crystal structure and triboluminescence 2. 9-anthracenecarboxylic acid and its esters. *Chem. Mater.* **9**, 1103–1105 (1997).
17. Rubin, I. B. & Buchanan, M. V. Carbon-13 NMR spectra of anthraquinone-derived dyes. *Magn. Reson. Chem.* **23**, 161–165 (1985).
18. Sakamoto, Y. *et al.* Structure-reactivity studies by NMR spectroscopy and molecular orbital calculation: nitration of polycyclic aromatic ketones. *Polycycl. Aromat. Comp.* **14–15**, 77–86 (1999).
19. Exner, O., Fiedler, P., Buděšínský, M. & Kulhánek, J. Conformation and steric effects in mono- and dimethoxybenzoic acids. *J. Org. Chem.* **64**, 3513–3518 (1999).
20. Hansen, P. E., Poulsen, O. K. & Berg, A. ^{13}C , ^{13}C coupling constants and ^{13}C chemical shifts of aromatic carbonyl compounds. Effects of *ortho*- and *peri*-interactions involving the carbonyl substituent. *Org. Magn. Resonance* **9**, 649–658 (1977).
21. Chaikin, S. W. & Brown, W. G. Reduction of aldehydes, ketones and acid chlorides by sodium borohydride. *J. Am. Chem. Soc.* **71**, 122–125 (1949).
22. Stankovich, S. *et al.* Synthesis of graphene-based nanosheets via chemical reduction of exfoliated graphite oxide. *Carbon* **45**, 1558–1565 (2007).
23. Schniepp, H. C. *et al.* Functionalized single graphene sheets derived from splitting graphite oxide. *J. Phys. Chem. B* **110**, 8535–8539 (2006).
24. Witter, R. *et al.* ^{13}C chemical shift constrained crystal structure refinement of cellulose I $_{\alpha}$ and its verification by NMR anisotropy experiments. *Macromolecules* **39**, 6125–6132 (2006).
25. Miyoshi, T., Hu, W. & Hagihara, H. Local packing disorders in a polymer crystal by two dimensional solid-state NMR. *Macromolecules* **40**, 6789–6792 (2007).
26. Verel, R., Manolikas, T., Siemer, A. B. & Meier, B. H. Improved resolution in ^{13}C solid-state spectra through spin-state-selection. *J. Magn. Reson.* **184**, 322–329 (2007).
27. Cadars, S. *et al.* The refocused INADEQUATE MAS NMR experiment in multiple spin-systems: interpreting observed correlation peaks and optimising lineshapes. *J. Magn. Reson.* **188**, 24–34 (2007).
28. Holland, G. P., Jenkins, J. E., Creager, M. S., Lewis, R. V. & Yarger, J. L. Quantifying the fraction of glycine and alanine in β -sheet and helical conformations in spider dragline silk using solid-state NMR. *Chem. Commun.* 5568–5570 (2008).
29. Kovtyukhova, N. I. *et al.* Layer-by-layer assembly of ultrathin composite films from micron-sized graphite oxide sheets and polycations. *Chem. Mater.* **11**, 771–778 (1999).
30. Hummers, W. S. & Offeman, R. E. Preparation of graphite oxide. *J. Am. Chem. Soc.* **80**, 1339–1339 (1958).
31. Mukherjee, A. *et al.* Dodecylated large fullerenes: an unusual class of solids. *Chem. Mater.* **20**, 5513–5521 (2008).

Acknowledgements

The authors (P.M.A., L.C., W.G.) acknowledge the support from the Interconnect Focus Center, one of five research centers funded under the Focus Center Research Program, a Semiconductor Research Corporation program. The authors also thank James M. Tour, Ashley Leonard, and Sun Zhengzong for helpful discussions and instrumental support.

Author contributions

W.G. and L.B.A. designed and performed the experiments and analysed the data. L.B.A. was responsible for all the NMR experiments and analysis. L.C. contributed materials, analysis tools and prepared the graphical abstract. W.G., L.B.A. and P.M.A. co-wrote the paper. P.M.A. was responsible for project planning. Correspondence and requests for materials should be addressed to P.M.A.

Additional information

Supplementary information accompanies this paper at www.nature.com/naturechemistry. Reprints and permission information is available online at <http://npg.nature.com/reprintsandpermissions/>. Correspondence and requests for materials should be addressed to P.M.A.